separations

MDPI

Article

Modified Polyethersulfone Ultrafiltration Membrane for Enhanced Antifouling Capacity and Dye Catalytic Degradation Efficiency

Mingming Wang [1], Feiyun Sun [1,2], Haojie Zeng [1], Xiaoli Su [1], Guofei Zhou [1], Hao Liu [1] and Dingyu Xing [1,*]

[1] Shenzhen Key Laboratory of Water Resource Utilization and Environmental Pollution Control, Harbin Institute of Technology, Shenzhen 518055, China; mm-ong@foxmail.com (M.W.); sun_fy@hit.edu.cn (F.S.); zenghj68@163.com (H.Z.); suxiaolihit@126.com (X.S.); zhouguofei2022@163.com (G.Z.); sqzzfb@outlook.com (H.L.)

[2] State Key Laboratory of Urban Water Resource and Environment, Harbin Institute of Technology, Harbin 150090, China

* Correspondence: xingdingyu@hit.edu.cn; Tel.: +86-755-26624592; Fax: +86-755-26032718

Abstract: Catalytic membranes, as a combination of heterogeneous advanced oxidation and membrane technology reaction systems, have important application prospects in the treatment of dyes and other organics. In practical applications, it is still challenging to construct catalytic membranes with excellent removal efficiency and fouling mitigation. Herein, molybdenum disulfide-iron oxyhydroxide (MoS_2-FeOOH) was fabricated using iron oxide and MoS_2 nanoflakes, which were synthesized by the hydrothermal method. Furthermore, by changing the concentration of MoS_2-FeOOH, the MoS_2-FeOOH/polyethersulfone (PES) composite ultrafiltration membrane was obtained with improved hydrophilicity, permeability, and antifouling capacity. The pure water flux of the composite membrane reached 385.3 L/(m^2·h), which was 1.7 times that of the blank PES membrane. Compared with the blank membrane, with the increase of MoS_2-FeOOH content, the MoS_2-FeOOH/PES composite membranes had better adsorption capacity and catalytic performance, and the membrane with 3.0% MoS_2-FeOOH content (M4) could be achieved at a 60.2% methylene blue (MB) degradation rate. In addition, the membrane flux recovery ratio (*FRR*) of the composite membrane also increased from 25.6% of blank PES membrane (M0) to more than 70% after two cycles of bovine serum albumin (BSA) filtration and hydraulic cleaning. The membrane with 2.25% MoS_2-FeOOH content (M3) had the best antifouling performance, with the largest *FRR* and the smallest irreversible ratio (R_{ir}). Catalytic self-cleaning of the composite membrane M3 recovered 95% of the initial flux with 0.1 mol/L H_2O_2 cleaning. The MoS_2-FeOOH/PES composite membranes with the functions of excellent rejection and antifouling capacity have a good prospect in the treatment of printing and dyeing wastewater composed of soluble dyes.

Keywords: catalytic self-cleaning membrane; antifouling; MoS_2; Fenton-like reaction

check for updates

Citation: Wang, M.; Sun, F.; Zeng, H.; Su, X.; Zhou, G.; Liu, H.; Xing, D. Modified Polyethersulfone Ultrafiltration Membrane for Enhanced Antifouling Capacity and Dye Catalytic Degradation Efficiency. *Separations* **2022**, *9*, 92. https://doi.org/10.3390/separations9040092

Academic Editor: Marco Brucale

Received: 10 March 2022
Accepted: 2 April 2022
Published: 4 April 2022

Publisher's Note: MDPI stays neutral with regard to jurisdictional claims in published maps and institutional affiliations.

Copyright: © 2022 by the authors. Licensee MDPI, Basel, Switzerland. This article is an open access article distributed under the terms and conditions of the Creative Commons Attribution (CC BY) license (https://creativecommons.org/licenses/by/4.0/).

1. Introduction

Ultrafiltration (UF) membranes have been widely used in water and wastewater treatment processes, including drinking water advanced treatment, seawater desalination and industrial wastewater reclamation [1–3], due mainly to their high efficiency, high selectivity, and wide application range [4–6]. However, reversible and irreversible fouling on porous membranes [7,8] inevitably decreases its permeability and service life [9,10], which significantly confines the application of UF membranes.

As a kind of advanced oxidation process (AOP), the Fenton method has obvious inherent advantages such as short reaction time, low cost, energy-saving, and environmental protection, which has been widely used in the field of sewage treatment [11]. Combined with this AOP, the catalytic membrane has become a candidate that is expected

to simultaneously separate particulate pollutants and degrade organic pollutants. Modified organic membranes such as polyvinylidene fluoride (PVDF) [12], polysulfone (PSF) [13] and polyethersulfone (PES) [14] have been reported, while modified inorganic membranes include ceramic membranes [15], carbon nanotubes [16], and molybdenum disulphide membranes [17]. The organic catalytic membrane process has the advantages of simple synthesis, low cost of raw materials, large-scale production, etc.

PES is one of the most common polymeric materials used in the synthesis of composite membranes for water engineering due to its high heat resistance, chemical stability, and good mechanical properties [18–20]. Recently, catalytic PES membranes combined with nano-sized catalytic materials, such as FeOCl, FeOOH, and Fe_3O_4/SiO_2, have been developed to give the membrane a certain catalytic ability [21]. For instance, a composite UF membrane was prepared by a coating nano-FeOCl catalyst, and had higher water flux and enhanced flux recovery about 100% by facile H_2O_2 cleaning on the membrane surface [22]. Chen et al. [23] incorporated iron phthalocyanine (FePc) into PVDF to fabricate the composite UF membrane (FePc loading of 2.5 wt%) that displayed an enhanced pure water flux and BSA rejection efficiency. However, the existing Fenton catalysts tend to aggregate due to their nanometer size, resulting in uneven catalyst distribution in the catalytic membrane, which may further lead to a reduced Fenton or Fenton-like efficiency and poor membrane performance [24,25]. Therefore, the synthesis of highly efficient and stable iron-based heterogeneous Fenton catalyst remains a challenge.

In recent years, FeOOH has had broad application prospects as a heterogeneous Fenton catalyst due to its abundant natural resources, low cost, and environmental friendliness. FeOOH also has high hydrophilicity and exhibits efficient catalytic activity for degrading contaminants through the Fenton reaction in the presence of H_2O_2. The catalytic function of the membrane can be achieved by mixing FeOOH with the membrane material. However, the agglomeration of FeOOH hinders its application. MoS_2 is one kind of good co-catalyst with excellent adsorption capacity, large specific surface area, and stable chemical stability [26]. MoS_2 is expected to avoid agglomeration of FeOOH and increase active exposure sites that could promote the reaction with reactants. Moreover, MoS_2 can also accelerate the reduction of Fe^{3+} to Fe^{2+} and thus increase the overall reaction rate. Hence, introducing MoS_2 as a co-catalyst in FeOOH-based catalytic membranes might continuously initiate oxidation for foulants removal.

In this study, a novel MoS_2-FeOOH/PES membrane was designed and prepared to simultaneously improve the membrane permeability and obtain the catalytic self-cleaning ability. The MoS_2-FeOOH nanoparticles were prepared and incorporated in the PES membranes during the nonsolvent-induced phase separation method. The adsorption and catalytic properties of the resultant membranes were investigated under different H_2O_2 content, pH, and pressures. In the filtration experiments of bovine serum albumin (BSA) solution and methylene blue (MB), oxidation-initiated membrane self-cleaning and degradation performance was evaluated with the addition of H_2O_2. In addition, antifouling mechanisms were analyzed by stepwise quenching trials on the catalyst, aiming to understand catalytic self-cleaning function for sustainable fouling mitigation. This method for contaminant removal and fouling control has potential for membrane application in water engineering.

2. Experimental

2.1. Materials and Reagents

Analytical grade chemicals were used for the catalytic membrane preparation without any further purification. Specifically, ammonium molybdate tetrahydrate ($(NH_4)_6Mo_7O_{24}\cdot 4H_2O$, 99%), thiourea ($CH_4N_2S$, 99.0%), and anhydrous ethanol (C_2H_6O, 99%) were obtained from Sinopharm Chemical Reagent Co., Ltd. (Shanghai, China). Ferric chloride hexahydrate ($FeCl_3$ $6H_2O$, 99.0%) and polyethylene glycol with an MW of 20,000 g/mol as porogen for membrane preparation were bought from Macklin Reagent Co., (Shanghai, China). Polysulfone (Mn 3000), N,N-dimethylacetamide (DMAC, $CH_3C(O)N(CH_3)_2$, 99.0%), and hydrogen peroxide (H_2O_2, 30 wt%) were obtained from Aladdin Biochemical Technology

Co., Ltd. (Shanghai, China). Methylene blue (MB, $C_{16}H_{18}C_lN_3S_3H_2O$, Aladdin) and bovine serum albumin (BSA, Sigma Aldrich) were used as the model pollutants for membrane filtration tests.

2.2. Synthesis of MoS_2-FeOOH Nanoparticles

MoS_2 nanosheets were fabricated by ammonium molybdate and thiourea using a one-step hydrothermal method according to a previous report [27], and the optimized preparation conditions included the molar ratio of Mo:S of 1:4, the hydrothermal temperature of 220 °C, and the hydrothermal time of 24 h. Upon the preparation of MoS_2 nanosheets, FeOOH was loaded onto MoS_2 to fabricate MoS_2 composite material according to previous research [28]. In addition, 0.16 g of MoS_2 and 3×10^{-4} mol of $FeCl_3$ $6H_2O$ were dispersed in 40 mL of absolute ethanol for 5 min. Furthermore, 0.158 g of NH_4HCO_3 was added to the mixed solution and stirred on a magnetic stirrer for 8 h. After the reaction, the catalyst was centrifugally washed with deionized water at 10,000 r/min for 3 times and dried under vacuum conditions for 24 h to obtain the MoS_2-FeOOH catalyst.

2.3. Preparation of MoS_2-FeOOH/PES Composite Membrane

MoS_2-FeOOH/PES composite UF membranes were synthesized by the phase inversion method in which the optimized MoS_2-FeOOH was blended [29]. In brief, the cast solution for membrane fabrication was comprised of 15% PES, 20% polyethylene glycol (PEG), and 65% DMA_C, which respectively took a role as a membrane material matrix, porogen, and solvent. At first, a predetermined amount of MoS_2-FeOOH was added into DMAc, and the formed mixture was dispersed homogeneously with the assistance of proper sonication. A certain amount of PEG, PES, and DMAc was then separately added into a flask and stirred thoroughly at 60 °C for 1.5 h in a water bath until the PES was fully dissolved. Afterward, the DMAc solvent containing MoS_2-FeOOH was homogeneously mixed and was added into the flask, which was then continuously stirred for 1.5 h until MoS_2-FeOOH was evenly dispersed in the casting solution. Subsequently, the obtained casting solution was left standing for 24 h until being completely degassed. Finally, the composite UF membranes were cast and immersed in water to remove excess solvent with the deionized (DI) water and refilled every 8 h for phase inversion. The prepared membranes were tested after 24 h of stabilization (Figure 1a).

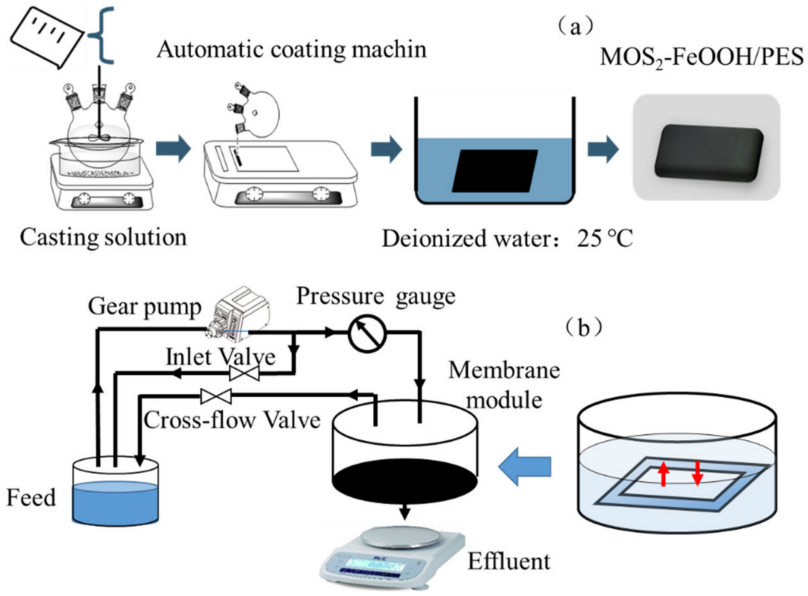

Figure 1. (**a**) Preparation procedure of MoS_2-FeOOH composite UF membranes; (**b**) schematic diagram of the cross-flow filtration set-up.

Four kinds of MoS_2-FeOOH/PES composite membranes with different compositions of MoS_2-FeOOH, including 0.05, 0.10, 0.15, and 0.20, were marked as M1, M2, M3, and M4, respectively (Table 1). A control membrane without MoS_2-FeOOH addition was also fabricated and characterized comparatively with composite membrane.

Table 1. Composition of the membrane casting solution.

Membrane Name	PES (%)	DMAc (%)	PEG (%)	MoS_2-FeOOH (%)
M0	15.00	65.00	20.00	0.00
M1	15.00	64.25	20.00	0.75
M2	15.00	63.50	20.00	1.50
M3	15.00	62.75	20.00	2.25
M4	15.00	62.00	20.00	3.00

2.4. Characterization of MoS_2-FeOOH Nanoparticles and Membranes

2.4.1. Characterization of Catalysts and Membranes

Scanning electron microscope (SEM, Hitachi SU8010, Tokyo, Japan) was used to study the morphology and microstructures of MoS_2-FeOOH nanoparticles (NPs) and MoS_2-FeOOH/PES composite membranes. X-ray photoelectron spectroscopy (XPS, Escalab 250Xi, Waltham, MA, USA) was used to analyze the chemical elements of the composite membrane. The major functional groups on the membrane were qualified by Fourier transform infrared spectrometer (FTIR, IRAffinity-1, Kyoto, Japan) with a resolution of 4 cm^{-1} and 32 scans. The crystal structure of MoS_2-FeOOH NPs was observed by powder X-ray diffraction (XRD, Bruker D8 Advance, Karlsruhe, Germany).

The water contact angles of MoS_2-FeOOH NPs and MoS_2-FeOOH/PES composite membranes were characterized using a contact angle measurement instrument (SL200 KB, KINO, Shanghai, China) with a video-based high-speed device at room temperature, and the data were analyzed with the Young–Laplace equation and CAST 3.0 software fitting method. Commonly, a water droplet was dropped on a dry membrane surface and the high-velocity video started recording. The average value was obtained from at least three different positions of each membrane, in order to indicate membrane surface hydrophilicity.

The gravimetric method was used to calculate the total porosity (ε) of obtained UF membrane [30]. The MoS_2-FeOOH/PES composite membranes were firstly placed in a 60 °C blast drying oven for 3 h to remove their moisture and then transferred into deionized water for 3 h until it was completely wet. The porosity of UF membranes was measured by weighing the dry and wet membrane following Equation (1):

$$\varepsilon = \frac{(m_1 - m_2)/\rho_w}{(m_1 - m_2)/\rho_w + m_2/\rho_m} \times 100\% \quad (1)$$

where m_1 and m_2 are the weight of the wet and dry membrane, respectively, ρ_w is the deionized water density (0.998 g/cm^3), and ρ_m is the composite membrane density (1.37 g/cm^3).

The average pore size of the membrane was measured by the filtration rate method using the Guerout–Elford–Ferry formula, which was calculated according to Equation (2) [31]:

$$r_m = \sqrt{\frac{(2.9, -, 1.75, \times, \varepsilon) \times 8\eta l J}{\varepsilon \times \Delta P}} \quad (2)$$

where ε and l are the membrane porosity and thickness, respectively, η is the viscosity of water (8.94×10^{-4} Pa·s), J is pure water flux (L/(m^2·h)), and ΔP is the applied transmembrane pressure (TMP) in the cross-flow filtration (0.1 MPa).

2.4.2. Permeability and Rejection Tests

Membrane filtration tests were carried out in a homemade cross-flow filtration setup (Figure 1b). The feeding solution was pressurized into the filtration cell by a gear pump and passed through the membrane under suction pressure, which was controlled by

adjusting the valve. The membrane was fixed in the membrane module with an effective filtration area of 19.6 cm^2. Constant TMP of 0.1 MPa during the filtration was kept for 90 min to run a filtration cycle, and the membrane flux was recorded by an electronic balance. The residence time (t, s) was adjusted by controlling the operating pressure and calculated using Equation (3) based on membrane thickness (ζ, μm) and membrane permeability (v, μm/s):

$$t(s) = \frac{\xi}{v} \tag{3}$$

The rejection efficiency, R (%), was then calculated according to the concentration of the target pollutant in feed and permeate solutions according to Equation (4):

$$R = \left(1 - \frac{C_p}{C_0}\right) \times 100\% \tag{4}$$

where C_p and C_0 are solute concentrations of permeate and feed solution, respectively.

2.4.3. Fouling Tests of the Membranes

The filtration-fouling test was conducted in the cross-flow filtration set-up, both TMP and membrane flux were recorded to indicate membrane fouling development. Bovine serum albumin (BSA) was used as a model organic foulant to evaluate the antifouling capability of the composite membrane. At a fixed room temperature and specific TMP, the pure water flux (J_w) and BSA permeate flux (J_P) were measured with the feed of pure water and 500 mg/L BSA solution, respectively. After the membrane fouled, the membrane was backwashed physically by DI water for 30 min, and the flux was marked as J_{wf}. Accordingly, flux recovery ratio (FRR), total fouling ratio (R_t), reversible ratio (R_r), and irreversible ratio (R_{ir}) were calculated by Equations (5)–(8) [14]:

$$FRR = \frac{J_{wf}}{J_w} \times 100\% \tag{5}$$

$$R_t = \left(\frac{J_w - J_p}{J_w}\right) \times 100\% \tag{6}$$

$$R_r = \left(\frac{J_{wf} - J_p}{J_w}\right) \times 100\% \tag{7}$$

$$R_{ir} = \left(\frac{J_w - J_{wf}}{J_w}\right) \times 100\% \tag{8}$$

2.5. Catalytic Characterization of Catalysts and Membranes

2.5.1. Catalytic Activity of the MoS_2-FeOOH

Methylene blue (MB), as one of the most common dyes, is a member of the thiazine family of dyes, and has been widely used in dye manufacture, food testing, organic synthesis, biological treatment, and other applications [31]. In this experiment, MB was used as a model organic contaminant to assess the catalytic activity of MoS_2-FeOOH NPs by degradation of MB molecules in an aqueous solution [32]. First, a desired amount of catalyst (MoS_2-FeOOH NPs) (0.0–1.2 g/L) was added to a 30 mL methyl blue solution of 40 mg/L, and mixed with a magnetic stirrer (IKA, BigSquid, Staufen, Germany) at room temperature. The catalyst was contacted with MB for 20 min to reach the adsorption–desorption equilibrium. After that, a certain amount of 30 wt% H_2O_2 solution was poured to conduct oxidation reaction to degrade MB, and the best dosage for the catalytic reaction was determined. No catalyst was added in the control experiment, while the rest steps were the same. The concentration of MB was determined by an ultraviolet-visible spectrophotometer (UV-2600, Shimadzu, Kyoto, Japan) at 664 nm absorbance. At different time intervals, 2.5 mL of suspension was extracted and filtered by a 0.22 μm filter to measure the concentration of residual MB concentration in the filtrate.

2.5.2. Catalytic Property of MoS_2-FeOOH Membranes

The Fenton-like catalytic performance of MoS_2-FeOOH membranes was evaluated by taking MB degradation rate as an indicator. In a typical process, a MoS_2-FeOOH membrane with an area of 2 × 5 cm^2 was placed flat in a 100 mL beaker, and 50 mL of MB solution (10 mg/L) were added. Keep the MB solution and membrane in a beaker for 20 min to reach adsorption equilibrium. Then, a certain amount of H_2O_2 aqueous solution (30 wt%) was added to provide hydroxyl radicals to initiate the reaction. During the reaction, 2 mL of MB solution were extracted at a certain interval, and then mixed with 2 mL of methanol to dilute the MB solution twice. In this process, the change of MB solution with time under the action of the membrane was investigated.

2.5.3. Filtration and Antifouling Performance of MoS_2-FeOOH Membranes

The blank and MoS_2-FeOOH/PES composite membranes were tested for dye removal efficiency at room temperature. The effective filtration area of the membrane was 19.6 cm^2. In addition, 5.5 L of MB (10 mg/L) and H_2O_2 (0.15 mol/L) mixed solution were pumped to permeate through the membrane, and the gear pump re-circulated the permeate solution to the feed solution. MB concentrations in the feed solution and permeate solution were measured at an interval of 5 min to evaluate MB removal efficiency. As a comparison, MB adsorption performances of membranes were also investigated under the same conditions except the addition of H_2O_2.

3. Results and Discussion

3.1. Characterization of MoS_2 and MoS_2-FeOOH Nanoparticles

The morphology of the original MoS_2 and MoS_2-FeOOH was shown in Figures 2a and 2b, respectively. MoS_2 had a layered structure with a smooth surface and uniform dispersion, with a size of about 300 nm. It can be seen from Figure 2b that there were many particles on the surface of MoS_2, which showed that FeOOH was successfully loaded on the surface of MoS_2. Furthermore, XRD was used to test the crystal structure of the original MoS_2 and MoS_2-FeOOH composite material. The results were shown in Figure 2c. It can be seen that the diffraction peak intensity and the full width of the original MoS_2 and MoS_2-FeOOH composites do not change significantly, indicating that the loading of FeOOH did not affect the crystal structure of MoS_2. Hence, FeOOH should be tightly fixed on the surface of MoS_2, without altering its structure. Figure 2d presented that the contact angle of the original MoS_2 and MoS_2-FeOOH corresponding 36.1° and 29.6°, respectively, indicating that the hydrophilicity of the catalyst MoS_2-FeOOH was enhanced by the doping of FeOOH. The contact angle of MoS_2-FeOOH was smaller than that of the original MoS_2, possibly because the addition of FeOOH has introduced OH functional groups which reduced the contact angle [33].

The effect of MoS_2-FeOOH concentrations on the degradation ability of organic dye MB was investigated. Firstly, the catalysts of different concentrations ranged 0.0 g/L to 1.2 g/L were added in the MB solution for 20 min to explore the adsorption effect, and then H_2O_2 was added for catalytic degradation experiments. As shown in Figure 2e, both the adsorption removal rate and degradation removal rate of MB gradually increased with the increase of catalyst concentration, and the total removal rates increased from 5.7% to 98.6%. The increase in catalyst concentration led to an increment in the number of exposed catalyst active sites, which could significantly improve the catalytic performance, thereby promoting MB degradation [34]. The stability and reusability of the catalyst were of great significance to its practical application. Thus, the reusability of MoS_2-FeOOH particles was investigated. The prepared MoS_2-FeOOH (1.0 g/L) and H_2O_2 (0.05 mol/L) were added into the 40 mg/L MB solution for catalytic degradation for 5 min, then centrifuged, washed, dried and recovered, and then put into the MB solution for the second round degradation. It can be seen from Figure 2f that the catalytic degradation activity of the sample decreased slightly with the increasing number of cycles. After four cycles, the catalytic degradation efficiency of MB dropped from 94.1% in the first cycle to 80.5% in the fourth cycle. The de-

crease in the catalytic activity of MoS_2-FeOOH particles may be owing to the particle loss during recovery, and slight poisoning and inactivation of particles during the degradation process [35].

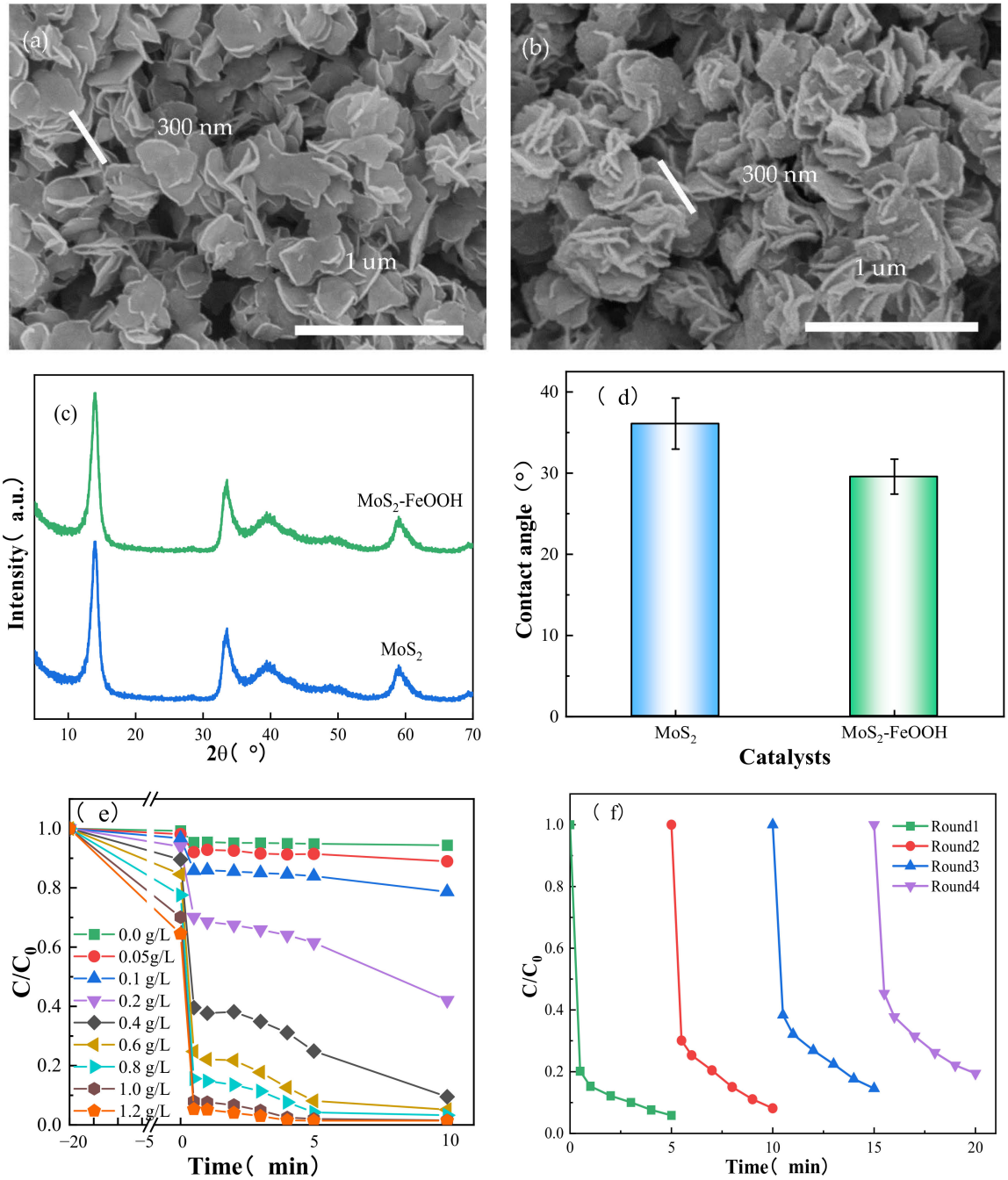

Figure 2. Characterization of the catalytic nanoparticles. (**a**) SEM image of MoS_2 nanoparticles; (**b**) SEM image of MoS_2-FeOOH nanoparticles; (**c**) XRD of MoS_2 and MoS_2-FeOOH nanoparticles; (**d**) water contact angle of MoS_2 and MoS_2-FeOOH nanoparticles; (**e**) MB degradation rate with different MoS_2-FeOOH nanoparticles content; (**f**) cyclic degradation of MoS_2-FeOOH nanoparticles.

3.2. Characterization of MoS_2-FeOOH/PES Composite Membranes

The MoS_2-FeOOH/PES composite membranes were fabricated according to the formulas in Table 1. Figure 3 showed the surface and cross-section structure of these catalytic membranes with different MoS_2-FeOOH contents. Compared with the PES membrane M0, all the MoS_2-FeOOH/PES composite membranes exhibited some particles on the surfaces

(Figure 2a M0-1-M4-1). Moreover, with the increase of MoS_2-FeOOH addition in the cast solution, there were clearly more particles deposited on the prepared PES membrane surface and pores, which confirmed the successful loading of MoS_2-FeOOH on/in the PES membrane matrix. The cross-sectional structure of the prepared membrane all displayed asymmetric finger-like structures, which was a typical UF membrane structural property.

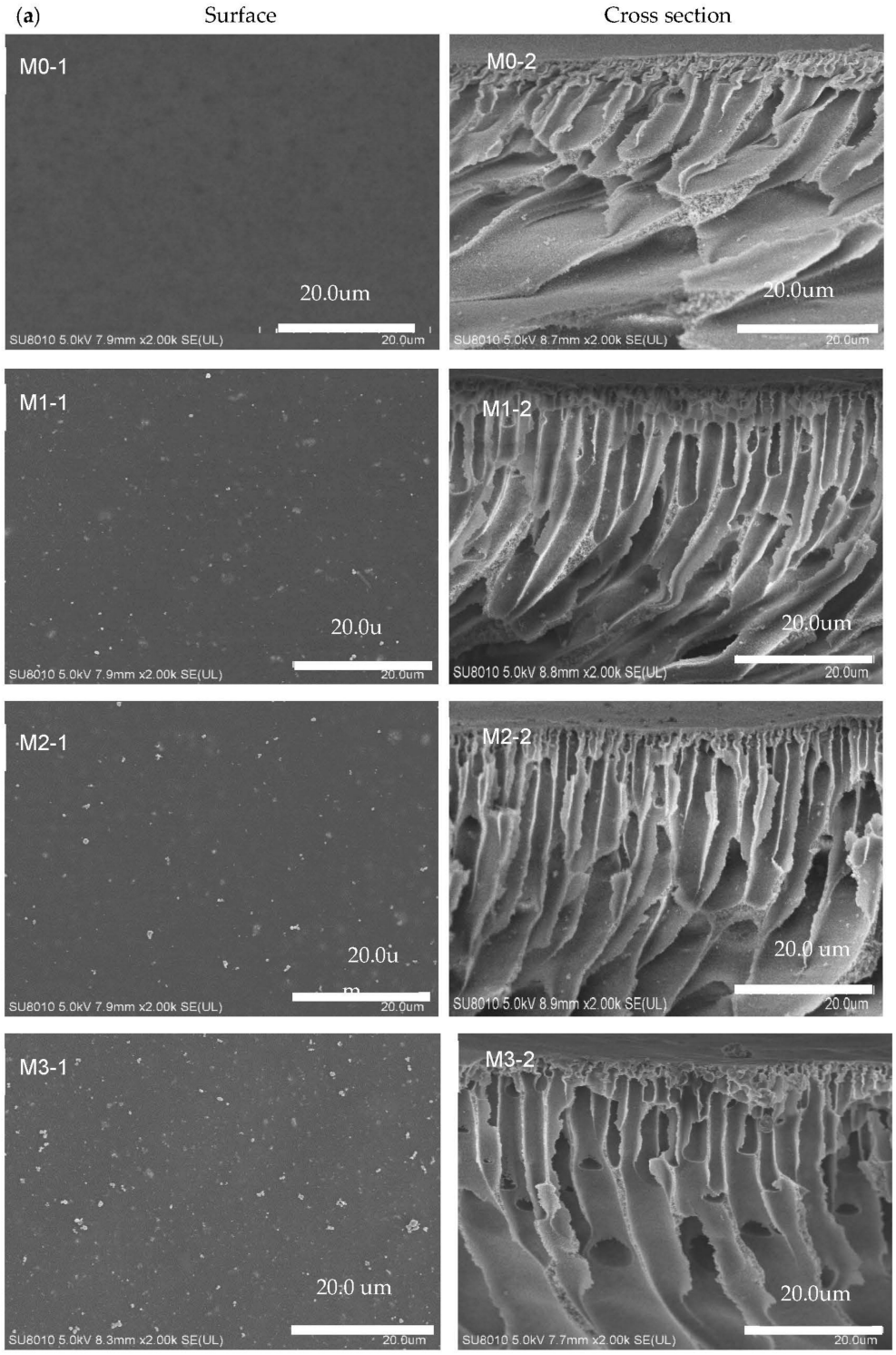

Figure 3. *Cont.*

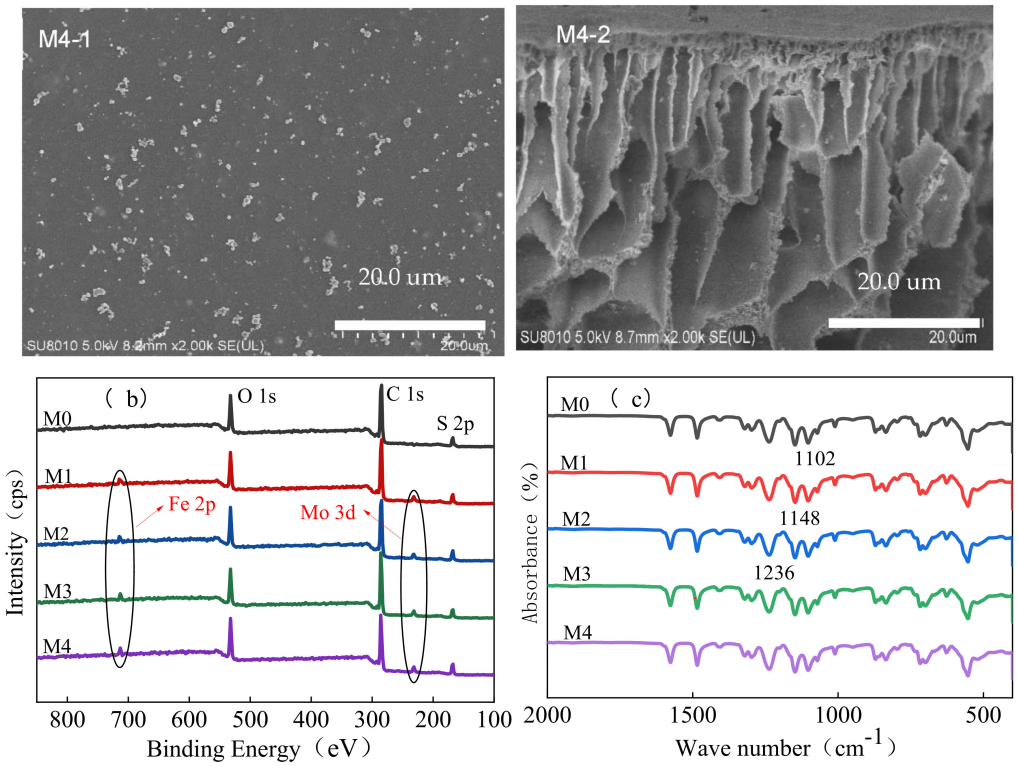

Figure 3. Characterizations of MoS_2-FeOOH/PES composite membranes (**a**) SEM images; (**b**) XPS spectra; and (**c**) infrared spectra.

The porosity and average pore size of the prepared membranes were summarized in Table 2. The MoS_2-FeOOH/PES membranes showed an increasing trend with the increment of MoS_2-FeOOH content, concurring well with the SEM observation. One reason was that MoS_2-FeOOH particles were more hydrophilic than PES, and in the process of phase separation, the diffusion of nonsolvent into the membrane pore and that of solvent from PES matrix would be accelerated. In addition, the introduction of nanoparticles would reduce the thermodynamic stability of the cast solution, which would also enhance the phase inversion rate and form a more porous structure [36]. Consequently, the MoS_2-FeOOH/PES composite membranes presented a slightly loose membrane structure with larger pores.

Table 2. Porosity and average pore size of membranes.

Membrane Type	Porosity (%)	Average Aperture (nm)	Contact Angle (°)
M0	77.6	27.0	49.2
M1	82.5	27.6	37.6
M2	83.5	28.8	35.1
M3	85.1	30.4	31.6
M4	85.8	31.6	34.3

XPS analysis of membrane surfaces in Figure 3b showed that, distinct from the control membrane M0, the binding energies peaks of 231.4 eV and 713.1 eV on the MoS_2-FeOOH/PES composite membranes were considered as the signal peak of Mo and Fe element, respectively. The phenomenon demonstrated that MoS_2-FeOOH was stably introduced into the PES matrix, corresponding well with the SEM images. The infrared spectra of all the MoS_2-FeOOH/PES composite membranes in Figure 3c displayed that the absorbance peak at 1102 cm^{-1} and 1148 cm^{-1} was mainly attributed to the stretching vibration of O=S=O, and the peak at 1236 cm^{-1} was due to the asymmetric stretching

vibration of C-O-C in PES polymer [37]. It was worth noting that MoS_2-FeOOH nanoparticles were mainly physically blending with PES, as no new peaks were found on the MoS_2-FeOOH/PES composite membranes.

From the water contact angle results of prepared membranes in Table 2, it was found that the introduction of MoS_2-FeOOH nanoparticles improved the membrane hydrophilicity, as the M1 with 0.75% MoS_2-FeOOH addition had a rather low contact angle of 37.6° that was rather improved compared to that of M0 of 49.2°. The increased dosage of hydrophilic MoS_2-FeOOH from 0.75% to 2.25% resulted in continuous improvement of membrane surface hydrophilicity [38]. However, with the increase of catalyst further to over 3.0%, excessive agglomeration of catalyst particles showed negative impacts on the membrane hydrophilicity [39]. Overall, it can be concluded that MoS_2-FeOOH nanoparticles have been successfully incorporated into the PES membrane with the enlarged pore size and enhanced surface hydrophilicity, which may promote the filtration and antifouling capability.

3.3. Ultrafiltration Performance of MoS_2-FeOOH/PES Composite Membranes

The pure water flux and BSA rejection efficiency of the MoS_2-FeOOH/PES composite UF membranes were evaluated under constant operating pressure of 0.1 MPa. As shown in Figure 4, all the MoS_2-FeOOH/PES composite membranes showed an enhanced BSA rejection efficiency compared to the PES membrane M0. With the increase of MoS_2-FeOOH content, the pure water flux of composite UF membranes increased significantly from 228 L/m^2·h to 385.3 L/m^2·h, due to the enhancement of the surface hydrophilicity and the increase of membrane porosity and average pore size. Meanwhile, the rejection efficiency of the BSA decreased slightly with the increment in the MoS_2-FeOOH dosage. Nonetheless, all the membranes had excellent BSA rejection efficiency ranging from 91.1% to 96.3%. It showed that the MoS_2-FeOOH/PES composite membranes have upgraded pure water flux and BSA rejection rate compared with some reports and commercial UF membranes [40].

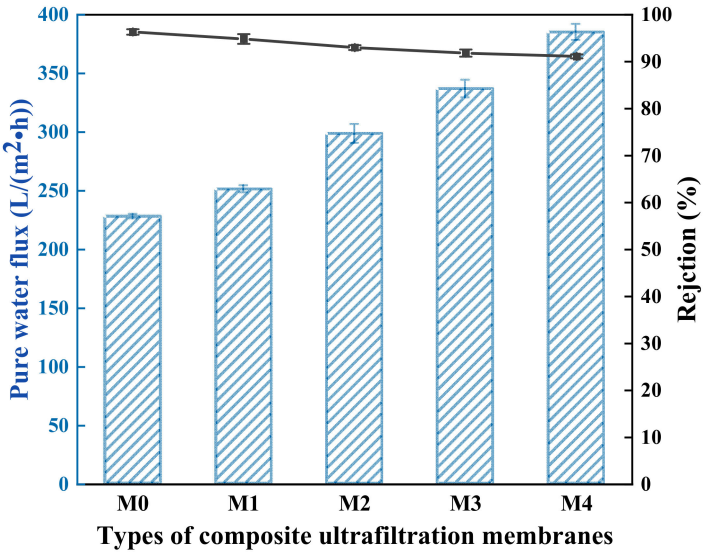

Figure 4. Pure water flux and BSA rejection for the MoS_2-FeOOH/PES composite membranes.

3.4. Catalysis Performance of the MoS_2-FeOOH/PES Membranes

The MB degradation by MoS_2-FeOOH/PES composite membranes was investigated in the presence of H_2O_2 according to the method in Section 2.5.2. It can be seen from Figure 5a that, compared with the PES membrane M0, the adsorption capacity of the composite catalytic membrane was obviously enhanced. In particular, M4 adsorbed nearly 20% MB before degradation, about 6.3 times that of M0 adsorption. There may be two reasons: on the one hand, new pore channels were formed due to the increased pore size and porosity of the composite membranes, thereby improving the adsorption capacity [41],

and on the other hand, the MoS_2-FeOOH catalyst showed adsorption effect as shown in Figure 2d. In the 180 min degradation experiment, it was found that the MoS_2-FeOOH/PES membranes could effectively decompose MB. In addition, as the content of MoS_2-FeOOH increased from 0.8% to 3.0%, the MB degradation efficiency increased from 24.1% to 60.2%, indicating that the addition of MoS_2-FeOOH enhanced the Fenton catalytic performance of the membrane. The more the MoS_2-FeOOH particles of composite membranes participated in the Fenton catalytic reaction, the more the hydroxyl radicals were generated and the higher the degradation efficiency [42]. During the catalytic process, the nanoparticles may escape from the MoS_2-FeOOH/PES composite membranes, and the released concentration of Fe was examined and shown in Figure 5b. Under neutral conditions, iron will not escape from the membrane. However, under acidic conditions, a small number of iron components would dissolve in the solution, and the leaching concentration increased with the amount of MoS_2-FeOOH. However, within the reaction time, the cumulative release of Fe was only 2.1 μg at most at pH = 4, which was relatively low compared to the iron content in groundwater, and had little impact on environmental health.

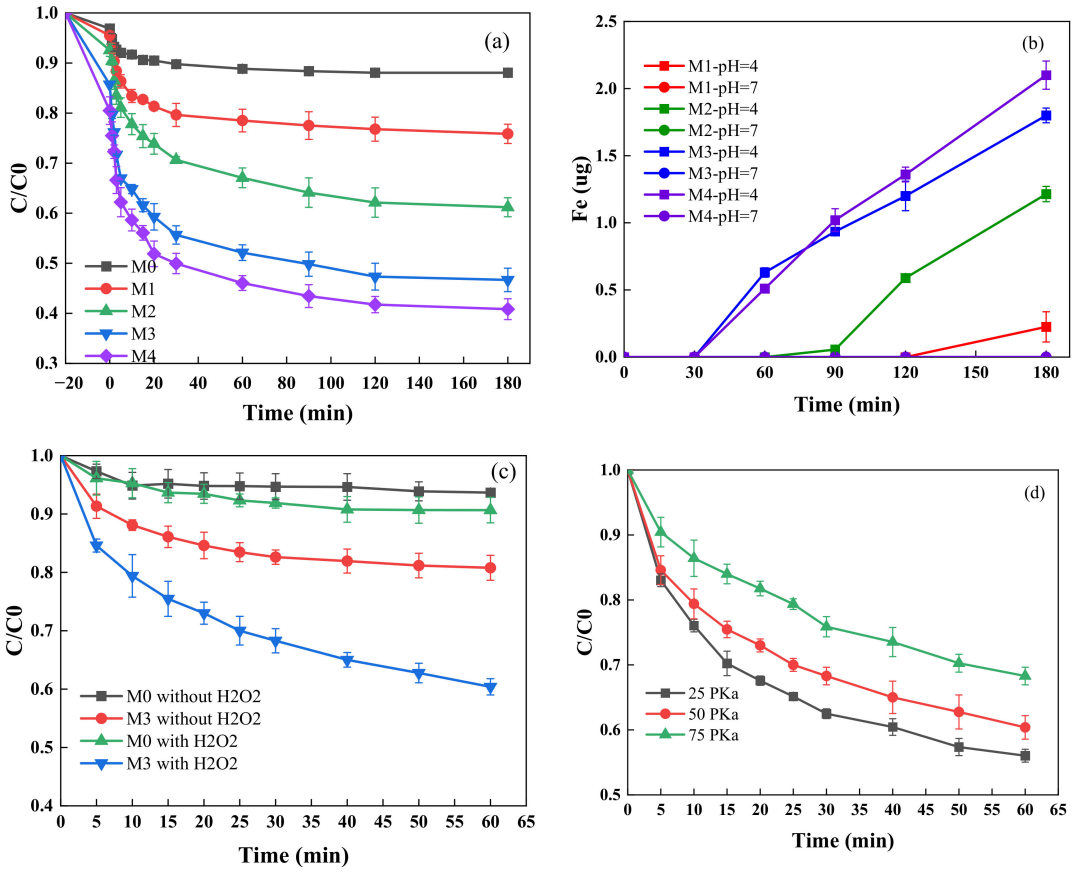

Figure 5. (**a**) Catalytic degradation effect of MB at pH = 4; (**b**) Fe release from the MoS_2-FeOOH/PES membranes at different pH; (**c**) degradation effect of MB in cross-flow filtration at 50 KPa; (**d**) degradation effect of MB in cross-flow filtration at 25, 50, and 75 PKa.

According to the results of Section 3.2, an M3 membrane with balanced properties was selected for testing the catalysis ability during the cross-flow experiment. The experimental results in Figure 5c showed that the MB removal rate of the PES membrane M0 did not change much with or without H_2O_2, and both were less than 10%. The degradation rate of M3 without H_2O_2 was close to 20%, which may be due to membrane interception and catalyst adsorption. After adding H_2O_2, the degradation rate of MB increased rapidly due to the Fenton effect. After 60 min, the degradation effect was 6.2 times and 4.2 times of the blank membrane with and without H_2O_2, respectively.

As indicated in Figure 5d, the lower the filtration pressure, the higher the MB removal efficiency by the M3 membrane, which indicated that a sufficiently long contact time is required to effectively adsorb and remove micro-pollutants. When the operating pressure was 25, 50, and 75 kPa, the membrane flux was 69.4 L/(m^2·h), 134.3 L/(m^2·h), and 193.7 L/(m^2·h). The residence time of MB in the membrane was 10.4 s, 5.4 s, and 3.7 s, respectively. When the operating pressure was 25 kPa, the residence time of pollutants in the membrane increased by about four times compared with that under 75 kPa, and the degradation rate increased by 1.39 times. These results show that reducing membrane flux and extending contact time can significantly improve the degradation effect of pollutants.

3.5. Antifouling Performance of Membranes with H_2O_2 Dosing

Using 500 mg/L BSA solution as the feed solution, two cross-flow filtration experiments were carried out after pressurizing pure water for 1 h, and their fouling evolution rate and flux recovery rate were compared. After each cycle of filtering the BSA solution for 1 h, the membrane was backwashed with deionized water for 30 min. It can be seen from Figure 6a that the initial pure water flux of MoS_2-FeOOH/PES membranes were all significantly higher in contrast to the M0 membrane, which was mainly due to the increase of the membrane surface hydrophilic groups, porosity and average pore size. After switching the feed to BSA, the water flux of the membrane dropped from 200–400 L/(m^2·h) to 50–150 L/(m^2·h), which mainly resulted from the BSA accumulation and adsorption on the membrane surface. After simple hydraulic cleaning, the pure water flux could only be partially restored, as there was irreversible fouling. Under the same filtration conditions, the pure water flux of all MoS_2-FeOOH/PES composite UF membranes was kept higher than that of the blank PES membrane. After two filtration cycles, these MoS_2-FeOOH/PES composite membranes displayed a consistently slower fouling rate than the control PES membrane. Especially for M3 and M4 membranes, after the second cycle, the flux was 4.6 times and 4.4 times that of M0, respectively.

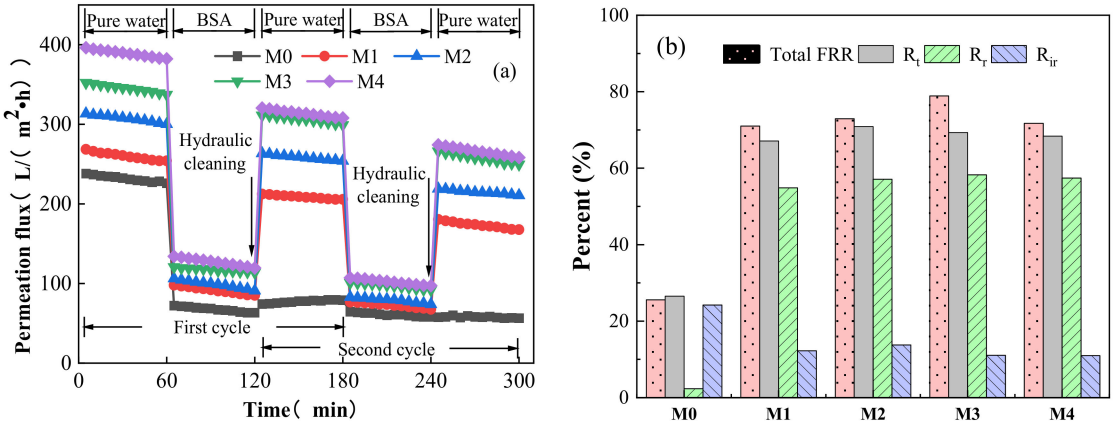

Figure 6. The antifouling performance for the filtration of BSA: (**a**) flux variation with the filtration process; (**b**) total *FRR* change during experiments and the fouling composition in the second cycle.

The fouling parameters, including *FRR*, R_t, R_r, and R_{ir}, were calculated according to the filtration-fouling tests. The higher the *FRR*, the better the antifouling performance of the membrane. Figure 6b illustrated that the *FRR* of M0 was much lower than that of MoS_2-FeOOH/PES composite membranes, and the *FRR* value of M1-M4 after two cycles were 2.8, 2.9, 3.1, and 2.8 times that of M0, respectively. It was observed that the flux recovery trend was consistent with the hydrophilicity of the membrane. In addition, M0 had the highest total fouling ratio R_t and irreversible ratio R_{ir}, and R_{ir} was the main component of R_t (up to ≥90%). Irreversible fouling cannot be removed by simple cleaning, so a smaller R_{ir} indicated that the anti-fouling capacity of the membrane had been improved. For the composite membranes, the R_t and R_{ir} were significantly reduced with the increase of MoS_2-FeOOH content, and the R_{ir} of M3 only accounted for 17% of the R_t. However, when

the amount of MoS_2-FeOOH added reached 3% (M4), the decrease of R_t and R_{ir} was not obvious. This result indicated that the antifouling capability of the prepared UF membranes were improved by adding MoS_2-FeOOH, but excessive catalyst could not further enhance its function. Overall, the membranes containing MoS_2-FeOOH composite exhibited higher antifouling performance compared to M0.

Afterward, M3 was employed to filtrate MB at 0.1 MPa, during which the permeation flux and flux recovery ratio were displayed in Figure 7. Throughout the experiment, the water flux of membrane M3 was always higher than M0, and the flux of the first and second filtration MB was about 1.8 times that of M0 membrane. After the first hour of membrane compaction, the feed was changed from pure water to MB, and a rapid drop in permeate flux was observed for both membranes. During the first MB filtration process, M3 had relatively smaller R_t (22.7%) and R_{ir} (11.7%). After the first cycle, membrane fluxes increased after hydraulic cleaning, and the *FRR* of M0 and M3 was 78.8% and 88.3%, respectively. In the second cycle, 0.1 mol/L H_2O_2 was used as the cleaning solution instead of pure water. For M0, H_2O_2 had little effect on flux recovery, while M3 had a significant improvement on flux, and the *FRR* can be increased to 95%. After the second round of MB filtration, the interaction between the catalyst in the membrane and H_2O_2, i.e., Fenton-like reaction, could generate •OH, which could effectively remove the reversible and irreversible pollutants on the membrane surface and membrane pores. Compared with M0, the irreversible fouling of M3 was significantly reduced to 5%, which indicates that the catalytic membrane has a better anti-fouling effect. The self-cleaning ability and stable performance of MoS_2-FeOOH/PES composite membranes could extend the membrane life about 15%, and has broad application prospects in the treatment of dye wastewater.

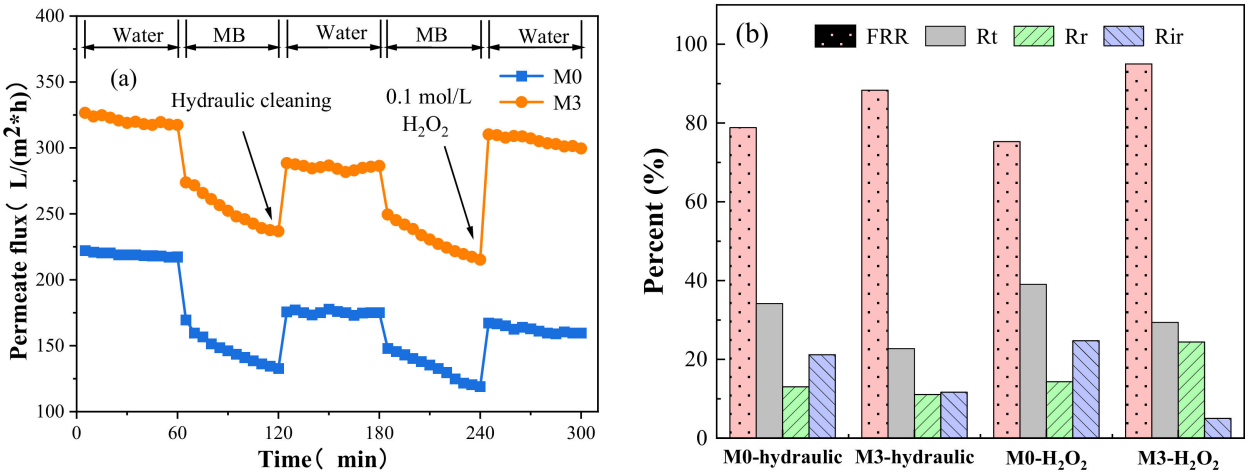

Figure 7. (**a**) Permeation flux of MB solution; (**b**) membrane fouling parameters with hydraulic cleaning or H_2O_2 cleaning.

Table 3 compares the MoS_2-FeOOH/PES membrane in this study with other works of PES membranes incorporating different nanomaterials for dye removal. As shown in the table, different types of inorganic nanomaterials have been used to improve PES membranes for increasing the resistance to various types of foulants and removing different dyes. This work endowed the composite membrane with the catalytic self-cleaning ability, thus presenting excellent water flux and antifouling capacity with reasonable dye rejection. Therefore, we expect that, by further adjusting the method of applying MoS_2-FeOOH, higher performance membranes can be produced for dye removal.

Table 3. Research done to improve composite PES membranes in dye wastewater treatment.

Polymer	Nanofiller	Flux ($Lm^{-2}h^{-1}$)	Rejection (%)	Goal	Refs.
PES	Cu(tpa)@GO	130 (0.18 MPa)	Congo Red ≥ 50 Methylene Blue <20	Antifouling and dye separation	[41]
PES	Fe_3O_4@SiO_2	2084 (0.1 MPa)	Methylene Blue =90	High-flux, antifouling and dye separation	[43]
PES	GO	289.63 (0.4 MPa)	Methylene read =67 Methylene orange =55 Congo read =95	Antifouling and dye separation	[44]
PES	TiO_2	142 (1 MPa)	Methylene Blue =30	Effective treatment of dye polluted wastewater	[45]
PES	MoS_2-FeOOH	385 (0.1 MPa)	Methylene Blue =60	High-flux, antifouling and dye separation	This work

3.6. Catalytic Self-Cleaning Mechanism in the MoS_2-FeOOH/PES System

MB was used to study its degradation mechanisms in MoS_2-FeOOH/PES membrane. The inhibition experiment of •OH was carried out to verify the role of •OH in the catalytic degradation of MB. Tert-butyl alcohol (TBA) was selected as a scavenger for the quenching test [46]. Figure 8a showed the effects of the capture agent on the catalytic performance after 20 min of static adsorption. After TBA was added, the removal efficiency of the MB was reduced from 98.1% to 31.5% after 10 min reaction, as MB was oxidized by •OH that was produced by MoS_2-FeOOH in the Fenton-like reaction. To verify this mechanism, DMPO was used as a free radical scavenger, and electron paramagnetic resonance (EPR) technology was used to identify active free radicals. Figure 8b clearly shows four characteristic peaks with an intensity ratio of 1:2:2:1, corresponding to the primary DMPO-·OH adduct.

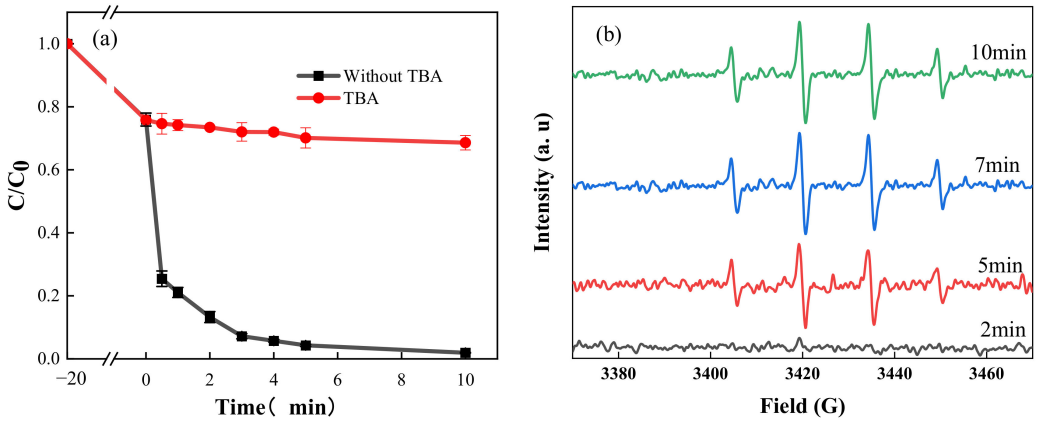

Figure 8. (**a**) Effect of TBA on MB degradation; (**b**) EPR spectra of DMPO–•OH.

The production paths of •OH were shown in Equations (9)–(12). Firstly, Fe^{3+} on FeOOH surface formed a surface complex Fe^{3+}–H_2O_2 with H_2O_2. In this complex, electron transfer occurred between Fe^{3+} and H_2O_2 to form $•O_2H$ and reduced Fe^{2+}, and the generated Fe^{2+} further reacted with H_2O_2 to form •OH [47]. During the whole heterogeneous Fenton-like process, the reduction of Fe^{3+} by H_2O_2 was the rate-limiting step [48]:

$$Fe^{3+} + H_2O_2 \rightarrow Fe^{3+}-H_2O_2 \quad (9)$$

$$Fe^{3+}\text{-}H_2O_2 \rightarrow Fe^{2+} + •O_2H + H^+ \quad (10)$$

$$Fe^{2+} + H_2O_2 \rightarrow Fe^{3+} + •OH + OH^- \quad (11)$$

$$Fe^{3+} + \bullet O_2H \rightarrow Fe^{2+} + O_2/H^+ \quad (12)$$

As shown in Equations (13) and (14), MoS_2 can promote the formation rate of Fe^{2+} from Fe^{3+}. Fe^{3+} in the solution was exposed to the active site Mo^{4+} of MoS_2 and reduced to Fe^{2+}. The regenerated Fe^{2+} ions could be redistributed into H_2O_2 aqueous solution to produce •OH. Meanwhile, the oxidized Mo^{6+} was reduced by H_2O_2 to form Mo^{4+} [49]:

$$Mo^{4+} + Fe^{3+} \rightarrow Mo^{6+} + Fe^{2+} \quad (13)$$

$$Mo^{6+} + H_2O_2 \rightarrow Mo^{4+} + H_2O + O_2 \quad (14)$$

In summary, the catalytic self-cleaning mechanism was summarized in Figure 9. The MoS_2-FeOOH/PES composite membrane could facilitate H_2O_2 to convert to •OH radicals by a Fenton-like reaction. The •OH radicals could further decompose dyes and other potential foulants such as BSA, resulting in an enhanced removal efficiency and antifouling capacity.

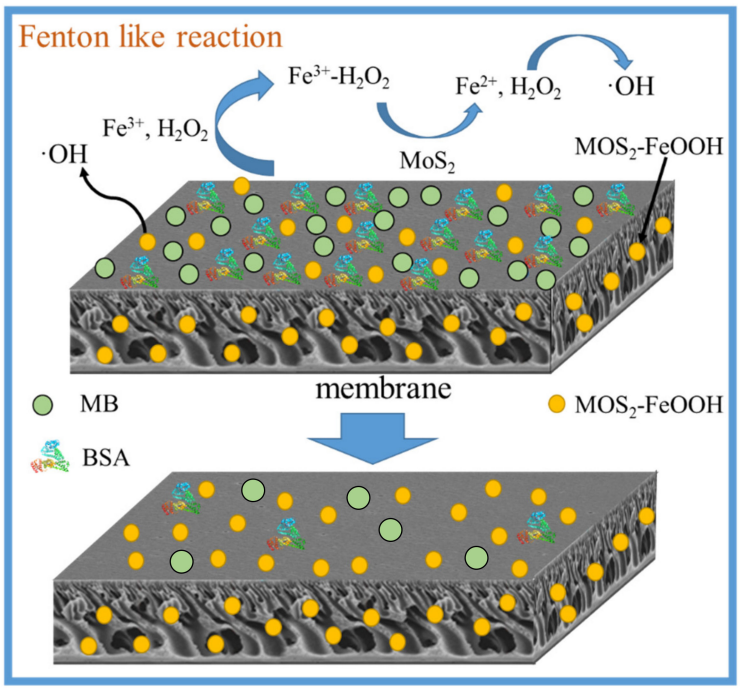

Figure 9. Schematic illustration of the catalytic self-cleaning mechanism.

4. Conclusions

In this study, a simple method was used to synthesize MoS_2-FeOOH and then the synthesized nanoparticles were mixed with PES casting solution to prepare a MoS_2-FeOOH/PES ultrafiltration composite membrane. XPS technology and infrared mapping confirmed that MoS_2-FeOOH was successfully introduced into the PES matrix by blending. It was found that the MoS_2-FeOOH/PES composite membranes showed a positive influence in porosity and hydrophilicity, increasing the permeability and the antifouling capability of the PES membrane. The composite membrane M3 had a balanced performance when the ultrasonic time was 1.5 h and the mass ratio of MoS_2-FeOOH to PES was 0.15. With the increase of MoS_2-FeOOH concentration, the pure water flux of the composite ultrafiltration membrane was gradually increased. The pure water flux of M3 was 337.0 L/(m^2·h), which was 1.5 times that of M0. In addition, antifouling experiments show that the BPA rejection rate of M3 was 91%, and the flux recovery ratio had increased from 25.6% of M0 to 78.9%. The irreversible resistance R_{ir} of the composite membrane was significantly reduced with the increase of added MoS_2-FeOOH content when the doping amount of MoS_2-FeOOH was less than 3%. M3 composite ultrafiltration membrane was

also used to treat dye simulated wastewater. It was found that the highest *FRR* of the M3 membrane could reach 95% after catalytic self-cleaning by H_2O_2, indicating that the composite ultrafiltration membrane has excellent antifouling performance and unique catalytic self-cleaning ability.

Author Contributions: Conceptualization M.W. and F.S.; methodology, H.Z.; formal analysis X.S. and G.Z.; investigation, M.W., G.Z. and H.L.; writing—original draft preparation, M.W.; writing—review and editing, F.S. and D.X.; supervision, F.S. and D.X.; project administration, F.S.; funding acquisition, D.X. All authors have read and agreed to the published version of the manuscript.

Funding: This research was supported by the National Natural Science Foundation of China (Grant Nos. 51808165, 52070053) and the Shenzhen Science and Technology Funding Project (Grant Nos. JCYJ20170816102318538, JCYJ20200109112825061, GXWD20201230155427003-0200824102301001, KCXFZ20201221173413036, KCXFZ202002011006362).

Conflicts of Interest: The authors declare no conflict of interest.

References

1. Sagbo, O.; Sun, Y.; Hao, A.; Gu, P. Effect of PAC addition on MBR process for drinking water treatment. *Sep. Purif. Technol.* **2008**, *58*, 320–327. [CrossRef]
2. Liu, M.H.; He, Q.Y.; Guo, Z.W.; Zhang, K.F.; Yu, S.C.; Gao, C.J. Composite reverse osmosis membrane with a selective separation layer of double-layer structure for enhanced desalination, anti-fouling and durability properties. *Desalination* **2021**, *499*, 114838. [CrossRef]
3. Lin, J.Y.; Huang, J.M.; Wang, J.; Yu, J.W.; You, X.Q.; Lin, X.C.; Van Der Bruggen, B.; Zhao, S.F. High-performance porous anion exchange membranes for efficient acid recovery from acidic wastewater by diffusion dialysis. *J. Membr. Sci.* **2021**, *624*, 119116. [CrossRef]
4. Rahimpour, A.; Madaeni, S.S.; Ghorbani, S.; Shockravi, A.; Mansourpanah, Y. The influence of sulfonated polyethersulfone (SPES) on surface nano-morphology and performance of polyethersulfone (PES) membrane. *Appl. Surf. Sci.* **2010**, *256*, 1825–1831. [CrossRef]
5. Werber, J.R.; Osuji, C.O.; Elimelech, M. Materials for next-generation desalination and water purification membranes. *Nat. Rev. Mater.* **2016**, *1*, 16018. [CrossRef]
6. Wang, W.Y.; Zhu, L.Y.; Shan, B.J.; Xie, C.C.; Liu, C.N.; Cui, F.Y.; Li, G.F. Preparation and characterization of SLS-CNT/PES ultrafiltration membrane with antifouling and antibacterial properties. *J. Membr. Sci.* **2018**, *548*, 459–469. [CrossRef]
7. Mokhtari, S.; Rahimpour, A.; Shamsabadi, A.A.; Habibzadeh, S.; Soroush, M. Enhancing performance and surface antifouling properties of polysulfone ultrafiltration membranes with salicylate-alumoxane nanoparticles. *Appl. Surf. Sci.* **2017**, *393*, 93–102. [CrossRef]
8. Pejman, M.; Firouzjaei, M.D.; Aktij, S.A.; Das, P.; Zolghadr, E.; Jafarian, H.; Shamsabadi, A.A.; Elliott, M.; Esfahani, M.R.; Sangermano, M.; et al. Improved antifouling and antibacterial properties of forward osmosis membranes through surface modification with zwitterions and silver-based metal organic frameworks. *J. Membr. Sci.* **2020**, *611*, 118352. [CrossRef]
9. Firouzjaei, M.D.; Shamsabadi, A.A.; Aktij, S.A.; Seyedpour, S.F.; Sharifian Gh, M.; Rahimpour, A.; Esfahani, M.R.; Ulbricht, M.; Soroush, M. Exploiting Synergetic Effects of Graphene Oxide and a Silver-Based Metal-Organic Framework to Enhance Antifouling and Anti-Biofouling Properties of Thin-Film Nanocomposite Membranes. *ACS Appl. Mater. Interfaces* **2018**, *10*, 42967–42978. [CrossRef]
10. Aghapour Aktij, S.; Zirehpour, A.; Mollahosseini, A.; Taherzadeh, M.J.; Tiraferri, A.; Rahimpour, A. Feasibility of membrane processes for the recovery and purification of bio-based volatile fatty acids: A comprehensive review. *J. Ind. Eng. Chem.* **2020**, *81*, 24–40. [CrossRef]
11. Wang, M.; Shu, Z.; Zhang, L.; Fan, X.; Tao, G.; Wang, Y.; Chen, L.; Wu, M.; Shi, J. Amorphous Fe^{2+}-rich FeO_x loaded in mesoporous silica as a highly efficient heterogeneous Fenton catalyst. *Dalton Trans.* **2014**, *43*, 9234–9241. [CrossRef]
12. Lin, H.; Fang, Q.; Wang, W.; Li, G.; Liu, F. Prussian Blue/PVDF Catalytic Membrane with Exceptional and Stable Fenton Oxidation Performance for Organic Pollutants Removal. *Appl. Catal. B Environ.* **2020**, *273*, 119047. [CrossRef]
13. Mukherjee, M.; De, S. Robust self cleaning polypyrrole-polysulfone blend hollow fiber membrane for biofouling mitigation. *J. Chem. Technol. Biotechnol.* **2018**, *93*, 3185–3198. [CrossRef]
14. Ko, K.; Yu, Y.J.; Kim, M.J.; Kweon, J.; Chung, H. Improvement in fouling resistance of silver-graphene oxide coated polyvinylidene fluoride membrane prepared by pressurized filtration. *Sep. Purif. Technol.* **2018**, *194*, 161–169. [CrossRef]
15. Garcia-Ivars, J.; Durá-María, J.; Moscardó-Carre, O.C.; Carbonell-Alcaina, C.; Alcaina-Miranda, M.I.; Iborra-Clar, M.I. Rejection of trace pharmaceutically active compounds present in municipal wastewaters using ceramic fine ultrafiltration membranes: Effect of feed solution pH and fouling phenomena. *Sep. Purif. Technol.* **2017**, *175*, 58–71. [CrossRef]
16. Liu, Y.; Lin, Q.; Guo, Y.; Zhao, J.; Luo, X.; Zhang, H.; Li, G.; Liang, H. The nitrogen-doped multi-walled carbon nanotubes modified membrane activated peroxymonosulfate for enhanced degradation of organics and membrane fouling mitigation in natural waters treatment. *Water Res.* **2022**, *209*, 117960. [CrossRef]

17. Chen, Y.; Zhang, G.; Liu, H.; Qu, J. Confining Free Radicals in Close Vicinity to Contaminants Enables Ultrafast Fenton-like Processes in the Interspacing of MoS_2 Membranes. *Angew. Chem.* **2019**, *58*, 8134–8138. [CrossRef]
18. Rahimpour, A.; Madaeni, S.S.; Mansourpanah, Y. Nano-porous polyethersulfone (PES) membranes modified by acrylic acid (AA) and 2-hydroxyethylmethacrylate (HEMA) as additives in the gelation media. *J. Membr. Sci.* **2010**, *364*, 380–388. [CrossRef]
19. Hofman, M.; Pietrzak, R. Copper ions removal from liquid phase by polyethersulfone (PES) membranes functionalized by introduction of carbonaceous materials. *Chem. Eng. J.* **2013**, *215*, 216–221. [CrossRef]
20. Kallem, P.; Ibrahim, Y.; Hasan, S.W.; Show, P.L.; Banat, F. Fabrication of novel polyethersulfone (PES) hybrid ultrafiltration membranes with superior permeability and antifouling properties using environmentally friendly sulfonated functionalized polydopamine nanofillers. *Sep. Purif. Technol.* **2021**, *261*, 118311. [CrossRef]
21. Etemadi, H.; Fonouni, M.; Yegani, R. Investigation of antifouling properties of polypropylene/TiO_2 nanocomposite membrane under different aeration rate in membrane bioreactor system. *Biotechnol. Rep.* **2020**, *25*, e00414. [CrossRef]
22. Sun, M.; Zucker, I.; Davenport, D.M.; Zhou, X.; Qu, J.; Elimelech, M. Reactive, Self-Cleaning Ultrafiltration Membrane Functionalized with Iron Oxychloride Nanocatalysts. *Environ. Sci. Technol.* **2018**, *52*, 8674–8683. [CrossRef]
23. Chen, F.T.; Shi, X.X.; Chen, X.B.; Chen, W.X. An iron (II) phthalocyanine/poly(vinylidene fluoride) composite membrane with antifouling property and catalytic self-cleaning function for high-efficiency oil/water separation. *J. Membr. Sci.* **2018**, *552*, 295–304. [CrossRef]
24. Senthilnathan, J.; Younis, S.A.; Kwon, E.E.; Surenjan, A.; Yoshimura, M. An efficient system for electro-Fenton oxidation of pesticide by a reduced graphene oxide-aminopyrazine@3DNi foam gas diffusion electrode. *J. Hazard. Mater.* **2020**, *400*, 123323. [CrossRef]
25. Wang, Y.; Zhao, G.; Chai, S.; Zhao, H.; Wang, Y. Three-Dimensional Homogeneous Ferrite-Carbon Aerogel: One Pot Fabrication and Enhanced Electro-Fenton Reactivity. *ACS Appl. Mater. Interfaces* **2013**, *5*, 842–852. [CrossRef]
26. Chhowalla, M.; Shin, H.S.; Eda, G.; Li, L.J.; Loh, K.P.; Zhang, H. The chemistry of two-dimensional layered transition metal dichalcogenide nanosheets. *Nat. Chem.* **2013**, *5*, 263–275. [CrossRef]
27. Li, X.; Zhang, C.; Xin, S.; Yang, Z.-C.; Li, Y.; Zhang, D.; Yao, P. A Facile Synthesis of MoS_2/Reduced Graphene Oxide@Polyaniline for High-Performance Supercapacitors. *ACS Appl. Mater. Interfaces* **2016**, *8*, 21373–21380. [CrossRef]
28. Wang, X.; Zhang, S.; Gao, H.; Huang, Y.; Wang, X.; Hayat, T.; Li, J.; Xu, X.J. Ultrathin g-C3N4 nanosheets coupled with amorphous Cu doped FeOOH nanoclusters as 2D/0D heterogeneous catalysts for water remediation. *Environ. Sci. Nano* **2018**, *5*, 1179–1190.
29. Abdi, S.; Nasiri, M.; Yuan, S.S.; Zhu, J.Y.; Van der Bruggen, B. Fabrication of PES-based super-hydrophilic ultrafiltration membranes by combining hydrous ferric oxide particles and UV irradiation. *Sep. Purif. Technol.* **2021**, *259*, 118132. [CrossRef]
30. Sukitpaneenit, P.; Chung, T.-S. Molecular design of the morphology and pore size of PVDF hollow fiber membranes for ethanol–water separation employing the modified pore-flow concept. *J. Membr. Sci.* **2011**, *374*, 67–82. [CrossRef]
31. Nicewicz, D.A.; Nguyen, T.M. Recent Applications of Organic Dyes as PhotoredoxCatalysts in Organic Synthesis. *ACS Catal.* **2014**, *4*, 355–360. [CrossRef]
32. Yong, G.; Meng, H.; Mi, B. Membrane surface modification with TiO_2–graphene oxide for enhanced photocatalytic performance. *J. Membr. Sci.* **2014**, *455*, 349–356.
33. Chen, J.; Meng, X.; Tian, Y.; Wang, X.; Zhu, J.; Zheng, H.; Wang, L. Fabrication of a superhydrophilic PVDF-g-PAA@FeOOH ultrafiltration membrane with visible light photo-fenton self-cleaning performance. *J. Membr. Sci.* **2020**, *616*, 118587. [CrossRef]
34. Wang, Z.; Meng, C.; Zhang, W.; Zhang, S.; Yang, B.; Zhang, Z. Honeycomb-like holey Co_3O_4 membrane triggered peroxymonosulfate activation for rapid degradation of organic contaminants. *Sci. Total Environ.* **2022**, *814*, 152698. [CrossRef] [PubMed]
35. Huong Le, T.X.; Dumée, L.F.; Lacour, S.; Rivallin, M.; Yi, Z.; Kong, L.; Bechelany, M.; Cretin, M. Hybrid graphene-decorated metal hollow fibre membrane reactors for efficient electro-Fenton-Filtration co-processes. *J. Membr. Sci.* **2019**, *587*, 117182. [CrossRef]
36. Sun, H.; Tang, B.; Wu, P. Development of Hybrid Ultrafiltration Membranes with Improved Water Separation Properties Using Modified Superhydrophilic Metal–Organic Framework Nanoparticles. *ACS Appl. Mater. Interfaces* **2017**, *9*, 21473–21484. [CrossRef]
37. Fu, W.; Zhang, W. Chemical aging and impacts on hydrophilic and hydrophobic polyether sulfone (PES) membrane filtration performances. *Polym. Degrad. Stab.* **2019**, *168*, 108960. [CrossRef]
38. Wang, R.; Zhao, X.; Lan, Y.; Liu, L.; Gao, C. In situ metal-polyphenol interfacial assembly tailored superwetting PES/SPES/MPN membranes for oil-in-water emulsion separation. *J. Membr. Sci.* **2020**, *615*, 118566. [CrossRef]
39. Feng, H.; Liu, J.; Mu, Y.F.; Lu, N.; Zhang, S.L.; Zhang, M.; Luan, J.S.; Wang, G.B. Hybrid ultrafiltration membranes based on PES and MOFs @ carbon quantum dots for improving anti-fouling performance. *Sep. Purif. Technol.* **2021**, *266*, 118586. [CrossRef]
40. Mantel, T.; Benne, P.; Parsin, S.; Ernst, M. Electro-Conductive Composite Gold-Polyethersulfone-Ultrafiltration-Membrane: Characterization of Membrane and Natural Organic Matter (NOM) Filtration Performance at Different In-Situ Applied Surface Potentials. *Membranes* **2018**, *8*, 64. [CrossRef]
41. Makhetha, T.A.; Moutloali, R.M. Antifouling properties of Cu(tpa)@GO/PES composite membranes and selective dye rejection. *J. Membr. Ence* **2018**, *554*, 195–210. [CrossRef]
42. Wang, T.; Wang, Z.; Wang, P.; Tang, Y. An integration of photo-Fenton and membrane process for water treatment by a PVDF@$CuFe_2O_4$ catalytic membrane. *J. Membr. Sci.* **2019**, *572*, 419–427. [CrossRef]

43. Zhang, L.-P.; Liu, Z.; Faraj, Y.; Zhao, Y.; Zhuang, R.; Xie, R.; Ju, X.-J.; Wang, W.; Chu, L.-Y. High-flux efficient catalytic membranes incorporated with iron-based Fenton-like catalysts for degradation of organic pollutants. *J. Membr. Sci.* **2019**, *573*, 493–503. [CrossRef]
44. Wang, X.; Feng, M.; Liu, Y.; Deng, H.; Lu, J. Fabrication of graphene oxide blended polyethersulfone membranes via phase inversion assisted by electric field for improved separation and antifouling performance. *J. Membr. Sci.* **2019**, *577*, 41–50. [CrossRef]
45. Chakraborty, S.; Loutatidou, S.; Palmisano, G.; Kujawa, J.; Mavukkandy, M.O.; Al-Gharabli, S.; Curcio, E.; Arafat, H.A. Photocatalytic hollow fiber membranes for the degradation of pharmaceutical compounds in wastewater. *J. Environ. Chem. Eng.* **2017**, *5*, 5014–5024. [CrossRef]
46. Peller, J.; Wiest, O.; Kamat, P.V. Sonolysis of 2,4-Dichlorophenoxyacetic Acid in Aqueous Solutions. Evidence for •OH-Radical-Mediated Degradation. *J. Phys. Chem. A* **2001**, *105*, 3176–3181. [CrossRef]
47. Feng, J.; Chu, C.; Ma, Z. Fenton and Fenton-like catalysts for electrochemical immunoassay: A mini review. *Electrochem. Commun.* **2021**, *125*, 106970. [CrossRef]
48. Wang, N.; Zheng, T.; Zhang, G.; Wang, P. A review on Fenton-like processes for organic wastewater treatment. *J. Environ. Chem. Eng.* **2016**, *4*, 762–787. [CrossRef]
49. Xing, M.Y.; Xu, W.J.; Dong, C.C.; Bai, Y.C.; Zeng, J.B.; Zhou, Y.; Zhang, J.L.; Yin, Y.D. Metal Sulfides as Excellent Co-Catalysts for H_2O_2 Decomposition in Advanced Oxidation Processes. *Chem* **2018**, *4*, 1359–1372. [CrossRef]